JGR Oceans

RESEARCH ARTICLE
10.1029/2020JC016354

Influence of the Pacific-South American Modes on the Global Spectral Wind-Wave Climate

E. R. Echevarria[1,2,3], M. A. Hemer[1], N. J. Holbrook[2,3], and A. G. Marshall[3,4]

[1]CSIRO Oceans and Atmosphere, Hobart, Tasmania, Australia, [2]Institute for Marine and Antarctic Studies, University of Tasmania, Hobart, Tasmania, Australia, [3]Australian Research Council Centre of Excellence for Climate Extremes, University of Tasmania, Hobart, Tasmania, Australia, [4]Bureau of Meteorology, Hobart, Tasmania, Australia

Key Points:
- The influence of the Pacific-South American (PSA) modes on the global spectral wind-wave climate is analyzed
- The PSA modes are significantly correlated with the variability of modeled wave heights and directions in the south Pacific
- Composite wind anomalies for positive stages of PSA modes are shown to explain the observed correlation patterns

Correspondence to:
E. R. Echevarria,
emilio.echevarria@csiro.au

Citation:
Echevarria, E. R., Hemer, M. A., Holbrook, N. J., & Marshall, A. G. (2020). Influence of the Pacific-South American modes on the global spectral wind-wave climate. *Journal of Geophysical Research: Oceans*, *125*, e2020JC016354. https://doi.org/10.1029/2020JC016354

Received 28 APR 2020
Accepted 29 JUL 2020
Accepted article online 3 AUG 2020

Abstract In this study, we analyze the influence of the Pacific-South American modes (PSA-1 and PSA-2) on the global wind-wave climate using wave data derived from a WAVEWATCH III global wave hindcast. We apply an empirical orthogonal function analysis to daily-averaged directional wave spectra to extract the two main patterns of interannual wave spectral variability. These are related to changes in the wave spectral density levels (variability in the wave heights) and to rotations of the wave signal (variability in wave direction). The PSA-1 mode is positively correlated with the wave height variability in the southeast Pacific and negatively correlated in the Indian Ocean sector of the Southern Ocean. The PSA-2 mode presents a strong negative correlation with wave heights in the central South Pacific. Moreover, the PSA modes are significantly correlated with changes in modeled wave direction in the South Pacific region. Composite maps of wind anomalies during positive stages of PSA-1 and PSA-2 provide a compelling explanation for the observed correlation patterns. The methodology applied in this study is also used to assess the influence of other climate modes on the global wind-wave climate (namely, the Southern Annular Mode, Arctic Oscillation, North Atlantic Oscillation, El Niño/Southern Oscillation, and the Pacific North American mode). While our results are consistent with previous studies, we provide more clarity as to how different atmospheric modes influence the variability of specific components of the wave spectrum. Importantly, we assess how these climate modes would modulate the interannual variability of wave direction.

Plain Language Summary Different modes of atmospheric variability (such as El Niño/Southern Oscillation or the Southern Annular Mode) are known to influence the ocean wind-wave climate in many regions of the world and across different timescales. The Pacific-South American (PSA) patterns represent important modes of variability of the atmospheric circulation in the Southern Hemisphere. In this study we use results from an ocean wind-wave model to analyze how the PSA patterns influence the global wave field. We apply a methodology that allows us to study in detail changes in wave height and direction. Our results suggest that the PSA modes would be associated with wind anomalies that modulate the height and direction of swell waves generated in the Southern Ocean, particularly in the south Pacific. We also analyze other climate modes of variability and their influence on the wind-wave field. Our results are consistent with previous studies, and they suggest that the influence of the PSA modes on the wind-wave field is of the same order of magnitude as that of other climate modes.

1. Introduction

Surface wind-generated waves drive and modulate many ocean processes and have a significant impact on human activities. Various operations at sea, such as fishing, navigation, or recreational activities, require estimations and/or forecasts of the sea state. At the coast, waves can substantially contribute to the total sea level through wave-induced setup and wave run-up (Dodet et al., 2019), as well as modulate the long-term coastal stability through resuspension and transport of sediments. Waves also generate ocean turbulence and mixing, which promotes exchanges of heat, mass, and momentum with the atmosphere, therefore being a contributing component of the climate system (Cavaleri et al., 2012). For all these reasons it is important to understand the processes governing the variability of wind waves and their sources.

The wind-wave state of a given region can change in a matter of hours but also across timescales from daily to interannual and longer. Understanding the nature of these variations can help improve wave climate

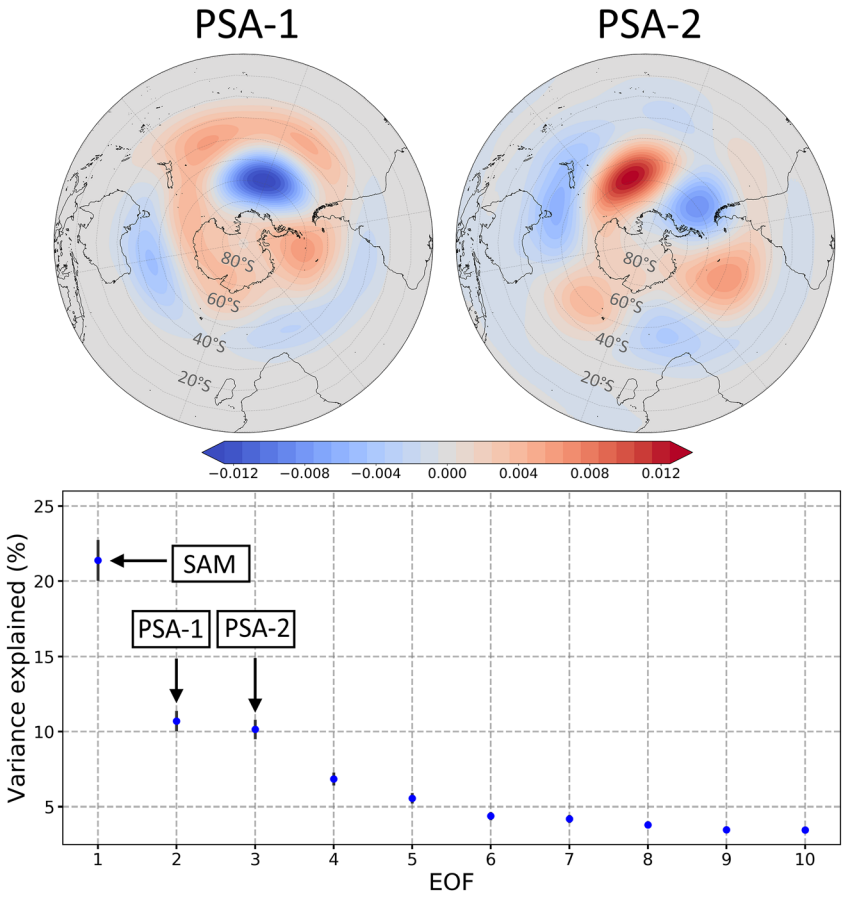

Figure 1. PSA-1 (top left) and PSA-2 (top right) patterns computed from monthly 500 mb geopotential height anomalies from 20°S to 70°S. Units are carried in the principal component time series. The eigenvalue spectrum is shown in the bottom figure.

predictability and provide a context for the study of wave trends and extreme values. The question of what drives interannual variability in the global wave field has been explored in several studies, and this knowledge has improved greatly in recent years, given the increasingly long record of wave observations (obtained remotely by satellites and in situ from buoys) and the development of global wind-wave model hindcasts and reanalyses. Large-scale modes of climate variability, such as El Niño-Southern Oscillation (ENSO), the Southern Annular Mode (SAM), and the Arctic Oscillation (AO), among others, are known to modulate interannual variations in surface winds and have an important influence on the global surface ocean wave climate (e.g., Hemer et al., 2009; Izaguirre et al., 2011; Marshall et al., 2015, 2018, 2020; Shimura et al., 2013; Stopa et al., 2013). This study focuses on the influence of the so-called Pacific-South American (PSA) modes on the wave climate.

The PSA modes represent one of the dominant atmospheric circulation features in the Southern Hemisphere. First identified by Mo and Ghil (1987), the PSA is characterized as an atmospheric Rossby wave train extending from south-eastern Australia to Argentina. It is somewhat analogous to the Pacific-North American (PNA) pattern (Wallace & Gutzler, 1981), hence its name. However, the PSA modes (or patterns) are defined with two patterns instead of one, namely, PSA-1 and PSA-2. They are usually defined as the second and third empirical orthogonal functions (EOFs) of 500-hPa geopotential height (GPH) (or 200-hPa streamfunction) monthly anomalies in the Southern Hemisphere, while the first EOF mode corresponds to the SAM. Importantly, the PSA-1 and PSA-2 modes are in quadrature and together depict the wave train. They are dominated by wavenumber 3 in midlatitudes, with largest amplitudes in the GPH field in the South Pacific sector of the Southern Ocean (Figure 1) and centers at approximately 60°S, 120°W (PSA-1) and 60°S, 90°W (PSA-2). They manifest in the intraseasonal to decadal time scales. It has been shown that the PSA

patterns play a significant role in atmospheric blocking events (Renwick & Revell, 1999) and in South American rainfall variability (Mo & Paegle, 2001). Importantly, they have been linked to the warming observed over West Antarctica and the Antarctic Peninsula (Marshall & Thompson, 2016) and to Antarctic precipitation variability (Marshall et al., 2017). Being such an important source of atmospheric circulation variability, the PSA patterns presumably exert a significant influence on the surface winds and, consequently, on the wind-wave climate of the South Pacific Ocean. However, this link has not yet been explored nor quantified. This paper aims to assess the influence of the PSA patterns, as well as other known large-scale climate modes, on the global wind-wave climate on interannual time scales and their potential consequences. A global wind-wave hindcast, together with an atmospheric reanalysis, is used to accomplish this.

Prior studies linking wave climate with modes of climate variability have typically explored the influence on bulk wave parameters (wave height and less so period or direction). As will be described in section 2.2, we make use of the full modeled directional wave spectra, enabling resolution of the response of the multimodal characteristics of the wave field with the patterns of climate variability.

This paper is organized as follows: Section 2 describes the wave hindcast data and the methodology to extract the patterns of spectral variability and defines and describes the PSA patterns and indices. Section 3 accounts for the results, showing the two main patterns of spectral variability of the global wave climate and their relationship to the PSA patterns (and other climate modes). Finally, a summary and discussion of the main outcomes are presented in section 4.

2. Data and Methods

2.1. The CAWCR Waves Hindcast

The Centre for Australian Weather and Climate Research (CAWCR), a partnership between the Australian Bureau of Meteorology (BoM) and the Commonwealth Scientific Industrial and Research Organisation (CSIRO), developed a long-term global wind-wave hindcast focused on the central and South Pacific (Durrant et al., 2013a, 2013b). It is an implementation of the third-generation spectral wind-wave model WAVEWATCH III® v4.08 (Tolman, 2009), forced with the Climate Forecast System Reanalysis (CFSR) 10 m winds and ice concentration (Saha et al., 2010) and its extension Climate Forecast System Version 2 (CFSv2). It provides hourly information of both integrated wave parameters (at resolutions ranging from 4 to 24 arc minutes) as well as directional wave spectra around the globe (with a spatial resolution of 10°) and around Australia and the Pacific Islands (with a resolution of 0.5°). Some of the most salient features of the model configuration are the Ardhuin et al. (2010) source term parameterizations; the Discrete Interaction Approximation (DIA, Hasselmann et al., 1985) for nonlinear wave-wave interactions; the third-order Ultimate Quickest propagation scheme (Leonard, 1979, 1991), including the garden sprinkler effect correction (Tolman, 2002); JONSWAP bottom friction, and Battjes and Janssen (1978) shallow water depth breaking. Besides, an increase of the sheltering term from 1.0 to 1.2 (related to an effective wind reduction by shorter waves) and decrease of the nondimensional growth factor of the input source term (βmax) from 1.52 to 1.33 were implemented, which improved the wave model performance in the Southern Ocean. Integrated parameters derived from the hindcast have been validated against observations and satellite data around the world, displaying a good performance of the model in terms of bias and root mean square error, and since its release this hindcast has been used in various wave studies (e.g., Gallop et al., 2014; Marshall et al., 2015, 2018; Rapizo et al., 2015). A comprehensive assessment of the skill of the CAWCR wave hindcast can be found in Durrant et al. (2014) for the whole globe and in Hemer et al. (2017) for the Australian region and therefore is omitted here.

The output of the CAWCR waves hindcast used in this study consists of hourly archives of directional wave spectra for 312 locations around the world, with a spatial resolution of 10°. The hindcast considers the varying sea ice concentrations, using the approach described by Tolman (2003). Hence, there are high-latitude grid points covered by ice during certain periods of the year, where no wave information is available. In order to ease the calculations, these ice-affected grid points were not considered in this analysis. The spectral frequencies in the model are discretized in 29 bins, varying exponentially from 0.038 Hz (26 s period) to 0.5 Hz (2 s period), and the directions were taken every 15°. While the CAWCR hindcast spans from 1979 through to near present, the selected time interval for this study spans from 1 January 1979 to 31 December 2019.

2.2. EOF Analysis Applied to Directional Wave Spectral Data

Usually, wave studies employ integrated parameters, such as significant wave height (Hs), mean period (Tm), or mean direction (θm) to characterize the wave climate. These values are computed through an integration of the wave spectrum, with the objective of reducing the information to a set of parameters (Hs, Tm, θm) that are representative of the average bulk wave climate. On the other hand, a directional wave spectrum describes how the waves' energy is distributed across frequencies and directions, hence providing the most complete description of the wave climate in a certain region, since it characterizes all the wave modes that may be present. Several authors (e.g., Echevarria et al., 2019; Hegermiller et al., 2017; Mortlock & Goodwin, 2015; Portilla-Yandún et al., 2016; Portilla-Yandún, 2018) outlined potential problems that could arise when describing the wave climate with integrated parameters. For example, defining the peak direction in cases where there are two independent swell modes will only consider the most energetic one and disregard the other. Considering the mean swell direction in the presence of opposing swell waves will not faithfully represent any of the wave components: For example, having two swell systems propagating to the southeast and northeast could yield an average direction to the east. This case may arise in the equatorial Pacific which receives swell waves from high-latitudes of both hemispheres (Echevarria et al., 2019; Semedo et al., 2011; Young, 1999). Likewise, the estimation of other wave parameters will be affected. Moreover, Portilla-Yandún et al. (2016) and Portilla-Yandún (2018) found that the presence of multiple swells and wind sea is rather common in most ocean basins. Therefore, these findings motivate us to employ an approach for the description of the wave climate that considers all possible wave modes.

We extend the methodology presented in Echevarria et al. (2019) to explore the main patterns of wave spectral variability on interannual time scales. EOF (e.g., Preisendorfer & Mobley, 1988) is commonly used in climate sciences to find dominant spatial patterns of variability of a certain climate variable, how this pattern changes through time, and the percentage of the total variance explained by these "modes." Most commonly, the EOF analysis is performed on spatially gridded data of a scalar quantity that fluctuates in time to find the geographic patterns that depict the main modes of variability of that quantity (e.g., Deser et al., 2010; Gulev & Grigorieva, 2006; for wave-related studies, see Hemer et al., 2009 or Semedo et al., 2011). Here, following Echevarria et al. (2019) and Shimura and Mori (2019), we employ a slightly different approach where the main modes of variability of the wave spectral density in the frequency/direction domain were obtained for each one of the spectral grid points of the model. These patterns represent the main modes of wave variability in the spectral domain, and the methodology allows us to analyze their temporal variability independently.

First, daily averages of the wave spectra at each grid point were computed. The model wave spectrum is expressed as $S(f_i, \theta_j, x_p, t)$, with f_i the frequencies ($i = 1$, ...,29 for the CAWCR hindcast), θ_j the directions ($j = 1$, ...,24), x_p the locations ($p = 1$, ...,312), and t the times (each day from 1 January 1979 to 31 Dec 2019). The daily averages were determined for each frequency/direction grid point and for each location separately. The daily annual cycle was computed (and removed from the data) using the 1979–2019 average spectra for each day of the year (the average for the 29 February was computed with the available 10 spectra only, but for the rest of the days 41 daily spectra were used to compute the average, one for each year in the record). Then, the data for each location were rearranged into a matrix containing the time series for each frequency/direction bin in the rows and each daily mean spectra in the columns (the dimensions of the matrix are 696 × 14,975; 696 = 29 frequencies × 24 directions and 14,975 = no. of days in the time period selected). The covariance matrix was next computed and the EOFs derived from it (see Echevarria et al., 2019 or Shimura and Mori, 2019 for a more detailed description and application of this methodology).

The EOFs represent the main patterns of variability in the wave spectral domain, and their temporal evolution is depicted by the principal component (PC) time series. For the correct interpretation of the results that will be shown in section 3, it must be kept in mind that the reconstruction of the original spectral data from a few EOFs is achieved as follows:

$$Reconstructeed\ spectra = \sum_i EOF_i * PC_i + S_{mean} \quad (1)$$

with PC being the PC time series, i the number of EOFs selected, and S_{mean} is the average spectra for each day of the year.

2.3. The PSA Patterns and Other Climate Indices

As explained earlier, the PSA patterns are defined as the second and third EOFs of the 500 mb (or hPa) GPH anomaly of the Southern Hemisphere, respectively (the first EOF corresponds to SAM). As such, they represent standing oscillations that are in quadrature, and their indices describe the temporal variability of the amplitude of these modes. Daily PSA-1 and PSA-2 indices from 1 January 1979 to 31 December 2019 were constructed using 500 mb GPH data taken from the CFSR and its extension CFSv2 (Saha et al., 2010). First, the PSA spatial patterns were computed as the second and third EOFs of the monthly averaged (instead of daily) 500 mb GPH anomalies from 20°S to 90°S, after removing the seasonal cycle and weighing the data by the cosine of the latitude. Then, daily GPH anomalies were projected onto these patterns to obtain the daily PSA indices. These daily indices were normalized by the standard deviation of the monthly indices. The signs of the PSA patterns were taken as those in Mo and Higgins (1998).

Other climate mode indices were also analyzed in this study: These included indices of the SAM (Limpasuvan & Hartmann, 1999), the AO (Thompson & Wallace, 1998), the North Atlantic Oscillation (NAO, Wanner et al., 2001), the ENSO (Philander, 1983) characterized by the NINO3.4 index, and the PNA mode (Wallace & Gutzler, 1981). The SAM, AO, NAO, and PNA daily indices from 1 January 1979 to 31 December 2019 and the NINO3.4 index from 1 September 1981 to 31 December 2019 were obtained from NOAA's Climate Prediction Center (http://www.cpc.ncep.noaa.gov).

3. Results

Daily mean spectra were computed for each day from 1 January 1979 to 31 December 2019 for each grid point, and the analysis described in section 2.2 was carried out to extract the main patterns of spectral variability (EOFs) and their temporal evolution (PCs). Section 3.1 presents maps of the first two EOFs (the most important spectral patterns of variability at each grid point), and section 3.2 shows the variance explained by these two modes of variability, to determine how many EOFs should be taken to attain an accurate reconstruction of the original values. Section 3.3 describes how the variability of these spectral patterns is modulated by the PSA modes. Finally, for completion and as a corroboration of the methodology, in section 3.4 other climate mode indices are analyzed for which their relationships to the wave climate have already been studied (namely, SAM, ENSO, AO, NAO, and PNA).

3.1. Principal Modes of Interannual Variability of the Wave Spectra

As described in section 2.2, at each spectral grid point the data set consisted of a sequence of daily mean directional wave spectra (from 1979 to 2019, with a total of 14,975 days), and the EOFs represent the patterns of spectral variability that arise from that sequence. This methodology was previously applied by Echevarria et al. (2019) at the global scale and by Shimura and Mori (2019) around Japan. Both studies found two distinct main patterns of spectral variability, which were also identified in this study. They will be hereafter labeled as "swell mode" and "rotation mode." The former describes the intensification/reduction of a wave signal in the spectra, typically a low frequency one, and the latter characterizes a change in the direction of that wave signal (see Figures 4 and 7 of Echevarria et al., 2019 and Figure 10 of Shimura and Mori, 2019).

The patterns depicted in EOF-1 are predominantly swell modes, and the rotation modes are contained mostly in EOF-2, although swell and rotation modes can also be found in higher-order EOFs. Figure 2 shows the global distribution of the swell modes. The dark red and blue tones correspond to EOF-1 and the light red and blue tones to higher-order EOFs that also represent a swell mode (a higher-order EOF was considered to be the secondary swell mode if its PC time series at that location was significantly correlated [$\alpha = 0.01$] with the PC time series of EOF-1 at neighboring locations, and with a correlation coefficient higher than 0.3. Swell modes were identified up to EOF-10). At high-latitudes of both hemispheres, these patterns show eastward propagating low frequency (swell) waves, resulting from the westerly winds that blow in this area. The EOFs represent the variation in their intensity throughout the years; that is, if the signal was constant in time, the EOF would not capture it. It can be observed how these swell waves propagate toward lower latitudes following great circle paths, shown as orange and green lines in Figure 2. At high-latitudes close to the wave generation area, the swell signals are broader, and once they disperse, they become more focused in

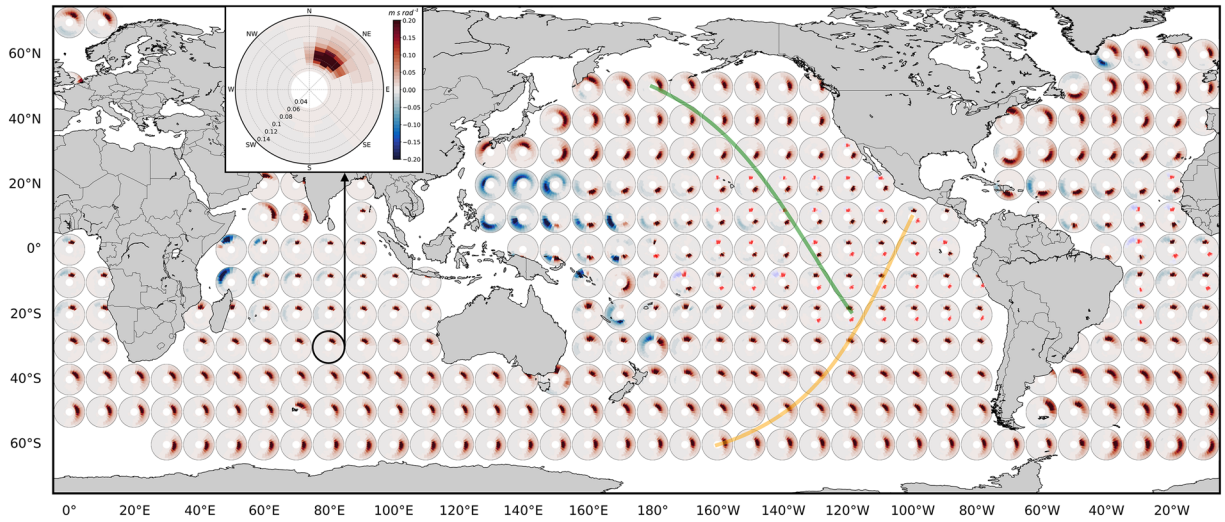

Figure 2. Principal modes of interannual spectra variability patterns (EOF-swell). The axis limits and the colorbar ranges are the same in every case and are shown for one location as reference. Directions are in oceanographic convention, that is, the direction waves propagate to. Dark red and blue tones correspond to EOF-1, while the light red and blue tones correspond to higher-order EOFs that are also considered to be swell modes.

one direction as they approach the equatorial regions. There is also a transition of the peak energy toward lower frequencies between the high-latitudes and equatorial waves, evidencing their dispersive behavior.

At low latitudes, particularly in the eastern Pacific, two swell modes were identified: namely, swell waves coming from the Southern Ocean and swell waves coming from the North Pacific. The variability of these two systems cannot be captured jointly in a single EOF; hence, one swell mode is captured by EOF-1, and the other mode is obtained in higher-order EOFs (shown in light red tones in Figure 2). These are the primary and secondary swell components. Figure 2 shows that these swell waves can coexist in a band of latitudes of approximately ±20° around the equator. In the North Indian Ocean, a higher frequency signal in the spectra emerges as a result of the variability of the surface winds produced by the Asian Monsoon. There is also faint evidence of the influence of the trade winds in equatorial regions, generating a relatively high frequency signal in the spectra. The sign of these patterns (EOFs) is meaningless in itself; whether a given pattern represents a positive or negative anomaly depends on the sign of the product of the EOF pattern and its corresponding PC time series (see equation 1).

Figure 3 shows the rotation modes, which are mostly captured in EOF-2. These patterns show positive and negative values at both sides of the main wave signal observed in the swell mode, representing a shift in spectral density from one direction to another. For example, in the North Pacific, most patterns in EOF-2 show negative values in the east direction and positive values in the southeast direction, which represents a clockwise rotation for positive values of the PC. At low latitudes, two rotation modes can be observed, one for each swell component (a higher-order EOF—other than EOF-2—was selected as the secondary rotation mode if its PC time series at that location was significantly correlated [$\alpha = 0.01$] with the PC time series of EOF-2 at neighboring locations and with a correlation coefficient higher than 0.3).

3.2. Variance Explained by Swell and Rotation Modes

The variance explained by the swell and rotation modes at each grid point is an important parameter for assessing the accuracy of the reconstructed data (Figure 4). The regions where the swell mode explains the highest amount of variance are located at high-latitudes, in the areas of most intense wave generation. It is greater than 50% in most areas of the Southern Ocean and the eastern North Pacific and Atlantic. It attains its lowest values in the equatorial regions and in the eastern sides of ocean basins. As to the variance explained by the rotation mode (Figure 4b), areas with relatively high values are found southwest of Australia and in the east Atlantic. In total, the variance explained by both EOF modes together is more than 70% in the Southern Ocean, East Indian Ocean, and North Pacific and Atlantic. On the other hand, in low latitude areas the variance explained by both EOFs is lower than 50%.

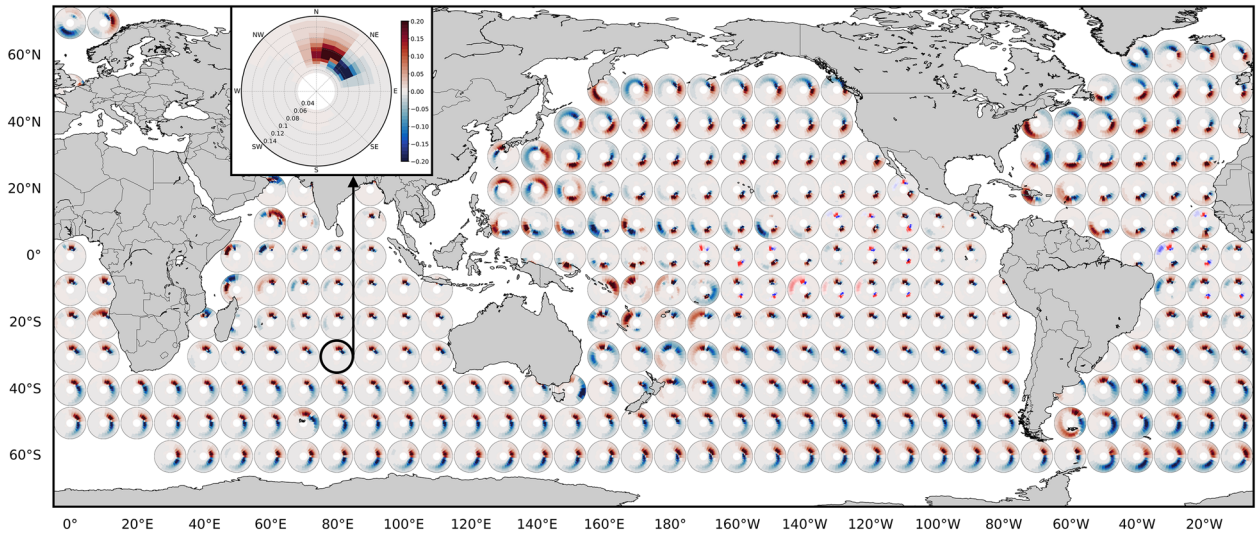

Figure 3. EOF-rotation patterns for the Pacific Ocean. Axis limits and colorbar range as in Figure 2. Dark red and blue tones correspond to EOF-2, while light red and blue tones correspond to higher-order EOF-s that are also considered rotation modes.

3.3. Influence of the PSA Patterns on the Spectral Wave Climate

The main aim of this work is to investigate the role that the PSA patterns have on the interannual variability of the global wave climate, in this case described through daily directional wave spectra. The temporal variability of the PSA patterns and the wave climate is described by the PSA indices and the PC time series of the EOFs, respectively. First, the PSA indices and PC time series (corresponding to the swell and rotation modes) at each location were detrended (to remove any possible spurious trend in the reanalysis data), and the Pearson's linear correlation between them was computed at each grid point. In the equatorial regions, where there are two swell modes present, we chose the mode corresponding to the Southern Ocean generated swell, since it was better correlated with the PSA indices. Additionally, the daily mean significant wave height (Hs) was computed using the original wave spectra at every grid point, and its anomalies were also correlated to the PSA indices to study the differences in both approaches. The Hs is computed by integrating the full wave spectrum over all frequencies and directions; hence, it is representative of the total wave energy contained in it, whereas the EOF patterns are representative of a single wave system in the spectrum. The comparison with the PSA indices is presented in Figure 5.

The patterns in Figure 5 show distinct (coherent) and statistically significant ($\alpha = 0.01$) relationships between the PSA modes and the wave climate of the South Pacific. The influences are primarily focused in the Southern Hemisphere but also extend into the Northern Hemisphere. The zonal wavenumber 3 feature that characterizes the PSA patterns can be identified in the correlation patterns of Figure 5. The PSA-1 pattern is positively correlated with wave heights in the eastern South Pacific extending to the equatorial regions and negatively correlated (although with less intensity) in the Tasman Sea and south of Australia. There is also a positive, albeit very low, correlation off Western Australia and a negative correlation in the South Atlantic. The PSA-1 also has an important apparent influence on the waves' rotation in the South Pacific, as evidenced by its positive correlation with PC-rotation in the central South Pacific and negative correlation south of Australia and Africa and south-westward of Chile. Considering Figure 3, this means that an anticlockwise rotation would develop in the central South Pacific, and a clockwise one around South Australia, South Africa, and Chile, during positive phases of PSA-1. The PSA-2 pattern, on the other hand, presents a strong negative correlation with the wave heights in the central South Pacific, also extending toward the equator. With less intensity, there is a negative correlation in the Indian and South Atlantic Ocean and a positive correlation in the Tasman Sea and along the Chilean coast and Drake Passage. The PSA-2 would produce an anticlockwise rotation of the waves in the eastern sector of the South Pacific that appears to be more intense than the one generated by PSA-1 pattern and an anticlockwise rotation around New Zealand. All correlations described are statistically significant at the 99% confidence interval.

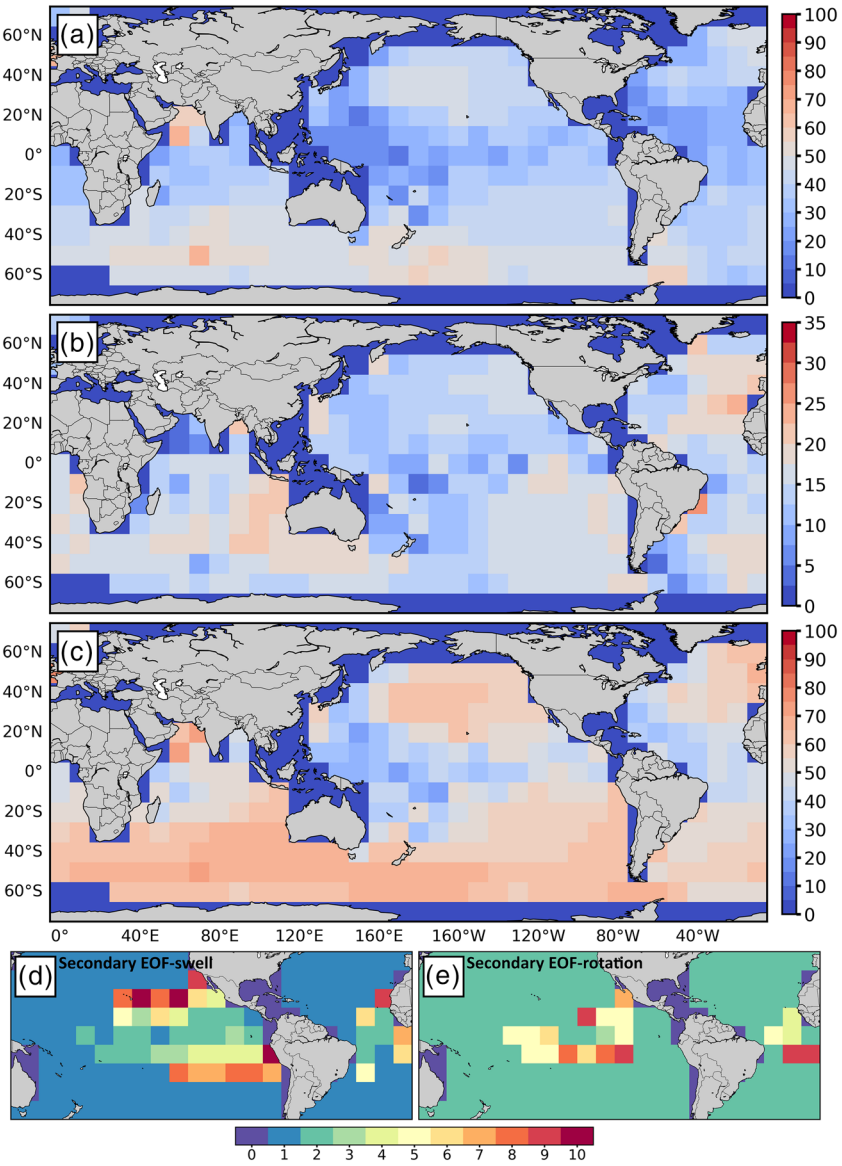

Figure 4. Variance explained by (a) EOF-swell, (b) EOF-rotation, and (c) EOF-swell and EOF-rotation together. In places where there are two swell or rotation modes, the variance was computed as the sum of the variances of the primary and secondary mode. (d) Higher-order EOF (other than EOF-1) that is also a swell mode. (e) Higher-order EOF (other than EOF-2) that is also a rotation mode.

To further understand the nature of the relationship between the PSA patterns and the wave climate in the Southern Hemisphere, composite maps of wind anomalies during positive phases or stages of PSA-1 and PSA-2 were calculated, using daily mean 10 m wind data from the CFSR reanalysis. Figure 6 shows the mean wind velocity and direction for the period 1979–2019 (upper panel) and the deviations from that mean state (wind anomalies) during positive phases of PSA-1 (middle panel) and PSA-2 (lower panel). Positive and negative phases of PSA-1 or PSA-2 were defined as those times where the corresponding daily PSA index was higher than one standard deviation and lower than minus one standard deviation, respectively.

The surface wind anomalies during positive stages of PSA-1 and PSA-2 are mostly a response to the GPH anomalies that characterize them. During positive phases of PSA-1, a clockwise circulation pattern develops, with its center at approximately 60°S, 90°W, which strengthens the predominantly westerly winds between 40°S and 60°S and weakens the winds south of 60°S. PSA-1 also appears to exert some influence on the

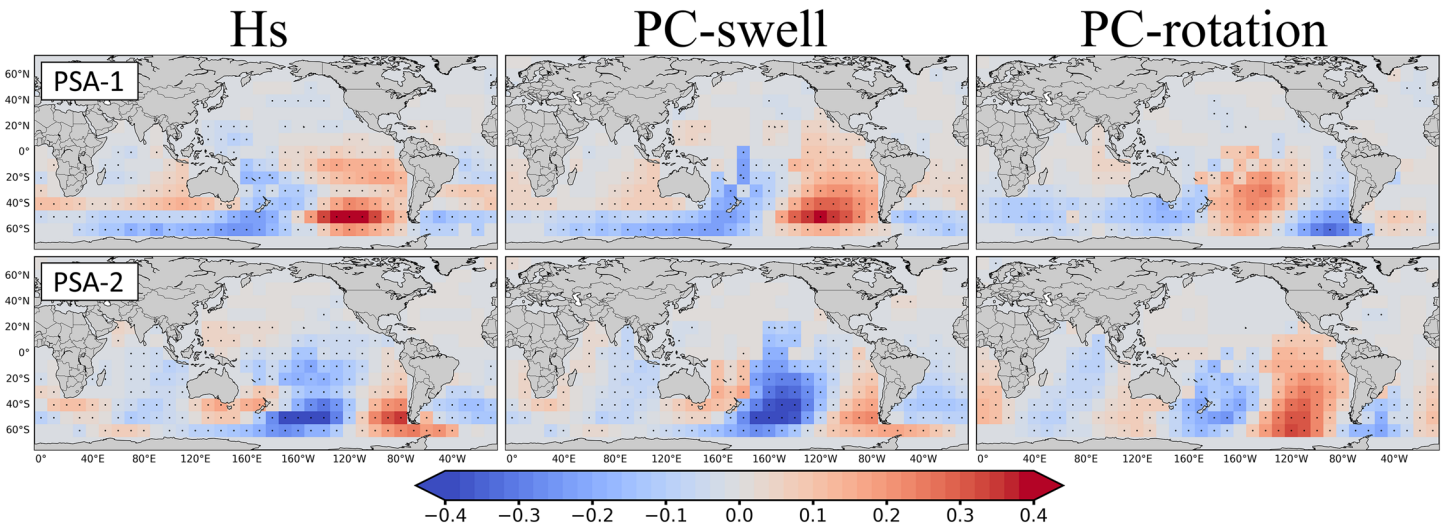

Figure 5. Upper panels: correlation between the PSA-1 index and Hs (left), PC-swell (middle), and PC-rotation (right). Lower panels: correlation between PSA-2 index and Hs (left), PC-swell (middle), and PC-rotation (right). Significant correlations at the 99% confidence level are marked with a black dot.

surface winds south of Australia and New Zealand. There is a mild positive correlation between the PSA-1 index and the wind intensity to the south-west of Australia and a negative correlation south of ~45°S which acts to reduce the westerlies intensity in this area. On the other hand, the most conspicuous characteristic of positive stages of PSA-2 is an anticlockwise circulation anomaly centered at 60°S, 120°W. The associated composite negative zonal wind anomalies between 40°S and 60°S result in less intense westerlies in the South Pacific, as it is observed in the strong negative correlation between PSA-2 index and the wind intensity south-eastwards of New Zealand. Southward of 60°S, there is a positive zonal wind anomaly which extends to South America and strengthens near the southwest coast of Chile. This positive wind anomaly would translate into more intense wave heights in this area, as Figure 5 suggests.

3.4. Influence of Other Climate Indices on the Spectral Wave Climate

Finally, we also compared the PC time series of the two main patterns of spectral variability (swell and rotation modes) with other climate mode indices: SAM, AO, NAO, NINO3.4, and PNA. As before, both the PC and climate index were detrended prior to the analysis, and the linear correlation coefficient between them was computed. For the equatorial regions, where there are two swell modes present, we selected the PC time series that best correlates with the climate index (for example, the SAM has a very strong relationship with the Southern Ocean swell, and therefore when correlating with the SAM index, this mode was selected instead of the Northern Hemisphere generated swell). The correlation distribution for each climate mode index with Hs, PC-swell, and PC-rotation is shown in Figure 7.

The SAM is the main driver of atmospheric variability in the Southern Hemisphere, influencing the strength and position of the westerly winds through changes in the pressure difference between the Antarctic continent and midlatitudes. There is a significant positive correlation between the SAM index and the daily mean Hs anomalies at high-latitudes of the Southern Ocean and in the South Pacific and negative correlations at midlatitudes of the Atlantic and Indian Ocean. The strongest relationship is found at high-latitudes of the Southern Ocean, southward of Australia and New Zealand. This is a consequence of shifts in the Southern Hemisphere storm belt during positive SAM phases, which generate positive and negative zonal wind anomalies at high- and midlatitudes, respectively. The maps of the correlation coefficient between SAM and the PC time series of the swell modes (PC-swell) show a similar distribution to that of Hs. However, the correlation with Hs decays toward lower latitudes, whereas the correlation with PC-swell is maintained approximately in the same values. This means that, at low latitudes, the SAM exerts its influence primarily on the Southern Ocean generated swell depicted by EOF-swell. Since Hs is representative of the total energy contained in the spectrum, it also considers high-frequency waves that are less affected (or not affected at all) by the SAM, and that is why the correlation values between SAM and Hs are lower.

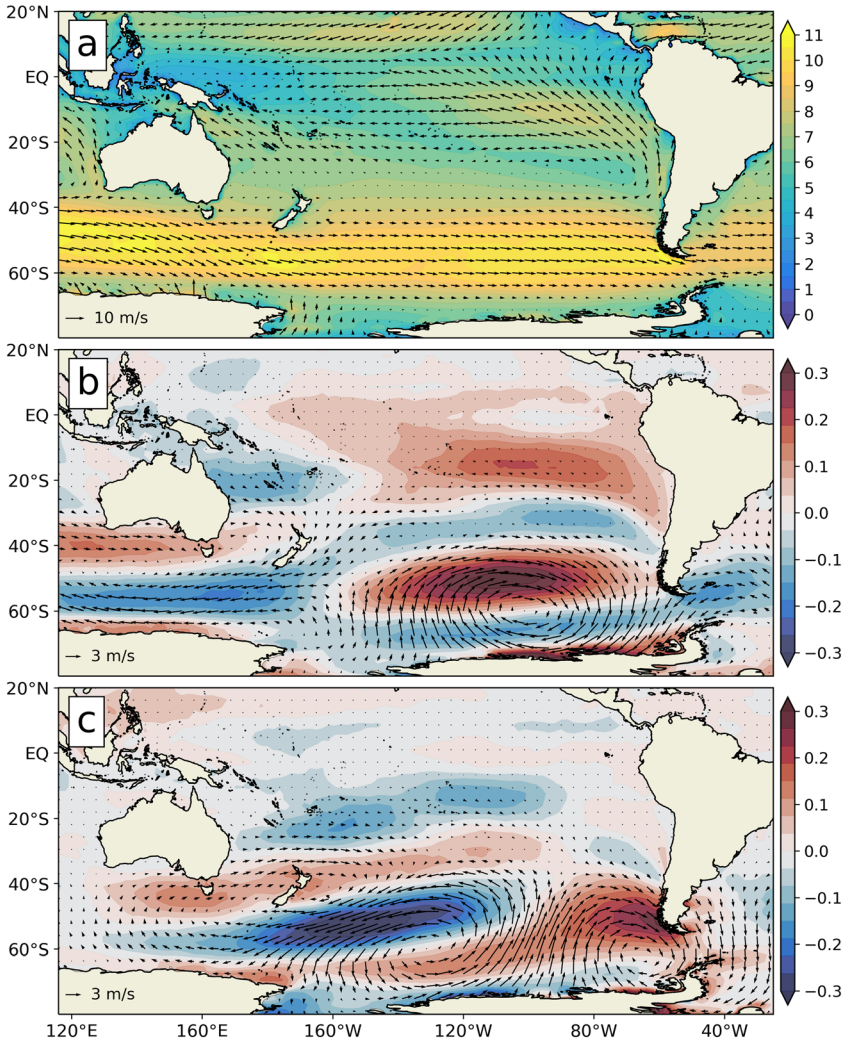

Figure 6. (a) Mean wind vectors for the period 1979–2019 and mean wind velocity in colors. (b and c) Arrows: wind anomalies during positive phases of PSA-1 (b) and PSA-2 (c). Colors: correlation coefficient between daily mean wind intensity and PSA-1 (b) and PSA-2 (c) index for the period 1979–2019.

The SAM also appears to have a widespread influence on the waves' rotation of the SH, especially southwest of Australia, as evidenced by the positive correlation between the SAM index and PC-rotation (the positive sign means that the rotation is anticlockwise for positive phases of SAM; see Figure 3).

Likewise, the main driver of atmospheric variability in the Northern Hemisphere is its corresponding annular mode, the AO. During positive phases of the AO, the westerly winds at high-latitudes of the Northern Hemisphere contract toward the Arctic, producing a dipole of positive and negative zonal wind anomalies at high- and midlatitudes, respectively. The strength and significance of the correlations between the AO index and PC-swell or Hs suggest that the atmospheric circulation anomalies developed as a consequence of the AO have an important influence on the wave climate of the Northern Hemisphere. Again, the correlation with Hs decreases toward lower latitudes while the correlation with PC-swell is maintained in approximately the same values as far as the equatorial regions. In this case, the eastern equatorial EOF pattern that was selected corresponds to the North Pacific generated swell mode, since it is the one that better correlates with the AO index. The AO is also significantly related to the rotation of the wave signal. Specifically, positive phases of the AO would correspond to a clockwise rotation in the east North Pacific and in the North Atlantic and an anticlockwise rotation in the West Pacific. The pattern of correlation with the NAO is similar to that with the AO but restricted to the Atlantic Ocean.

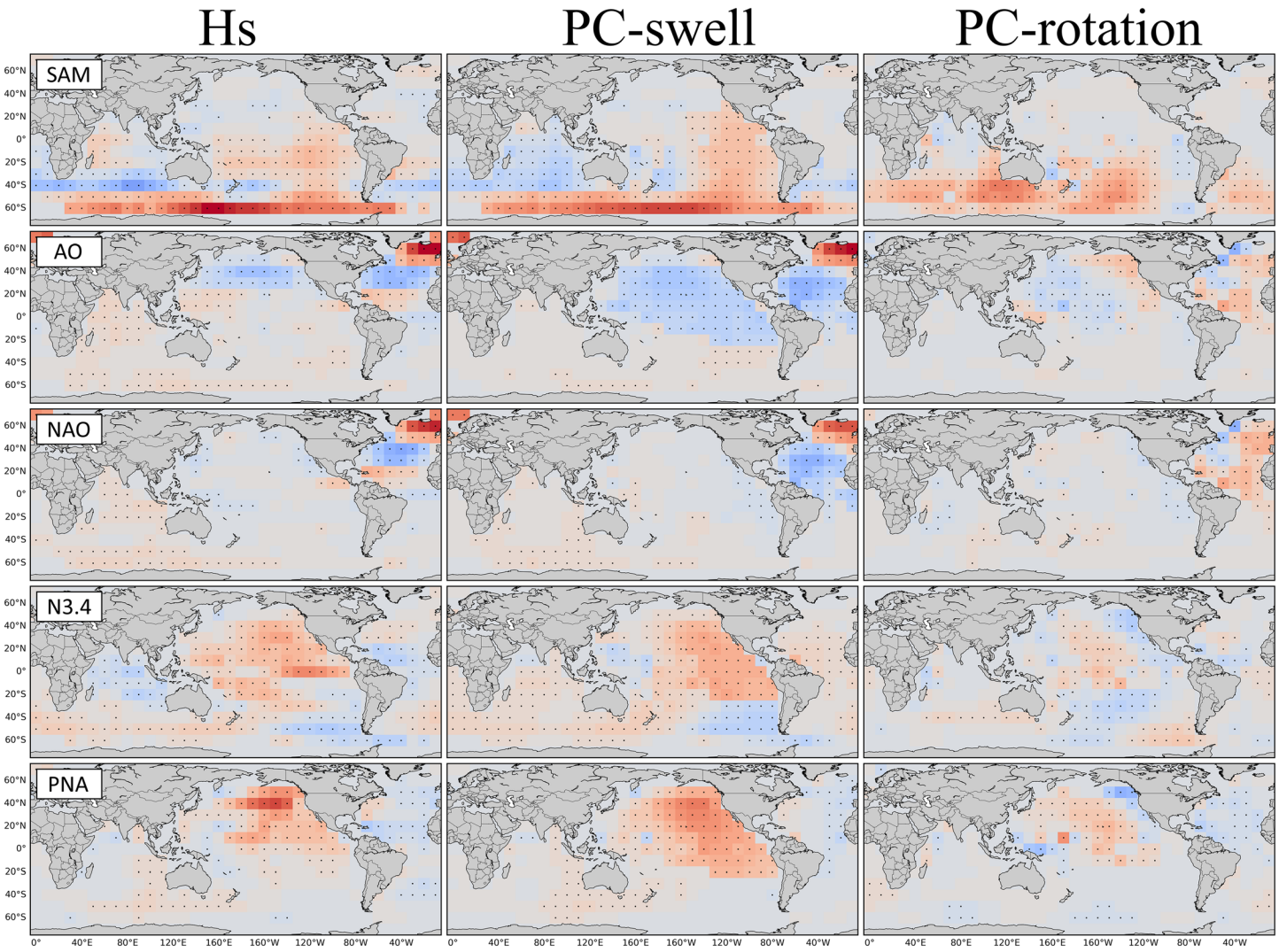

Figure 7. Distribution of the linear correlation coefficient between climate indices and the significant wave height (Hs) and PC-swell and PC-rotation. Significant correlations (at the 99% confidence level) are denoted with a black dot.

The relationship between ENSO and the wave field is complex across the Pacific Ocean and, to a lesser extent, in some areas of the Indian and Atlantic Ocean. During El Niño events (defined as prolonged periods of warm sea surface temperatures anomalies [>0.5°C] in the central equatorial Pacific, which correspond to positive NINO3.4 index values. See https://www.cpc.ncep.noaa.gov/), the easterly trade winds weaken and contract to the eastern equatorial Pacific, accompanied by a warming and consequent low sea-level pressure anomaly in this area. Further, teleconnections related to ENSO produce changes in the atmospheric circulation all around the world. During El Niño events, there tends to be an amplification and extension of the westerlies of the North Pacific toward the east, which translate into more intense wave generation. This is evidenced in Figure 7 by the positive correlation between the NINO3.4 index and Hs (or PC-swell) in this area and extending to the eastern equatorial Pacific. On the other hand, during La Niña events (defined as prolonged periods of cool sea surface temperature anomalies in the central equatorial Pacific, which correspond to negative NINO3.4 index values), a positive zonal wind anomaly tends to develop in the southeast Pacific (a strengthening of the westerlies), which translates into more intense wave generation in that area.

Finally, our results also suggest that the PNA has widespread influence on the waves in the eastern and central North Pacific. Positive phases of the PNA are associated with a deepening of the Aleutian Low and a consequent intensification of the westerly winds of the North Pacific, which in turn produce anomalously

higher waves. As to the correlation with PC-rotation, it shows low negative values (although statistically significant) in the North Atlantic and positive values in the western and central North Pacific. This means that during positive PNA phases, there is an intensification of the mean swell signals at high-latitudes of the Pacific Ocean accompanied by a clockwise rotation of those waves. The contrary happens in the North Atlantic but less markedly, that is, a reduction of the intensity and anticlockwise rotation of the eastward propagating waves.

4. Summary and Discussion

The approach outlined in Echevarria et al. (2019), and briefly described in section 2.2, was implemented in the present study to investigate the patterns of interannual wave spectral variability using daily averaged directional wave spectra from 1979 to 2019, taken from the CAWCR global wave hindcast data set. The time evolution of these patterns of spectral variability at each grid point was then compared to various climate mode indices to better understand the potential drivers of interannual variations in the global spectral wave climate. The motivation for using directional wave spectra as opposed to integrated parameters is founded on the potential loss of representativeness of the latter, as discussed by Portilla-Yandún (2018). We found that the PSA modes have a very strong and statistically significant (at the 99% level) connection with the South Pacific wave climate, suggesting that these modes play a very important and influential role in the region's wave climate, including along the coasts of New Zealand and Chile. Further, this methodology allowed us to separate the impact of different climate modes on different patterns of spectral variability (swell and rotation modes).

At high-latitudes of both hemispheres, the main mode of interannual daily wave spectral variability (EOF-1) corresponds to the variation of relatively low frequency (period of ~15 s) waves that propagate eastwards as a consequence of the intense westerly winds; these swell waves propagate equatorward following great circle paths, becoming an important source of interannual variability at midlatitude and low latitude. The second most important mode of variability (EOF-2) at high-latitudes represents a rotation of the main swell signals. Finally, EOF-3 describes a change in frequency of the observed wave signals, from lower to higher frequencies or vice versa depending on the sign of their PC (figures not shown). At low latitudes, the wave climate is more complex and multimodal: There is variability associated with swell waves coming from both hemispheres, with different time evolutions. Since both swell modes cannot be captured jointly in a single EOF, one mode is captured in EOF-1 and the other mode in higher-order EOFs. Likewise, there are "rotation" modes for the Northern and Southern Hemisphere swell modes, captured in EOF-2 and higher-order EOFs. To provide more clarity and consistency to our results, we decided to group all the "swell" modes in Figure 2 and the "rotation" modes in Figure 3.

The variance explained by EOF-swell is large at high-latitudes, in areas of intense wave generation (Figure 4). The eigenvalue spectrum (the distribution of variance explained across the EOFs) for these locations is very steep; that is, EOF-1 explains a significantly larger proportion of the variance than the remaining EOFs (figures not shown). The variance explained by the swell and rotation modes together is generally higher than 70% for latitudes greater than 20°, except in the western side of ocean basins. In the equatorial region, the variance explained by both modes reaches an average value of around 50%. The eigenvalue spectrum of these areas is relatively flat; that is, the variance explained by the first few EOFs is comparatively similar. Therefore, it should be considered that, in terms of data reconstruction, a different degree of accuracy was achieved at each model grid point.

Of all the climate mode indices considered in this study, PSA-1 and PSA-2 presented the highest values of correlation with daily time series of Hs or PC-swell in the South Pacific region. It is well-known that the Southern Ocean generated swell waves can travel across the Pacific, reaching as far as the coasts of Alaska (Gallet & Young, 2014; Munk & Snodgrass, 1957; Snodgrass et al., 1966). Our results suggest that the PSA modes could substantially modulate the generation, height, and direction of these swell waves. PSA-1 is positively correlated with the wave heights (as represented by Hs or PC-swell) in the eastern South Pacific and negatively correlated (although with less intensity) with wave heights in the Tasman Sea and in the Indian Ocean sector of the Southern Ocean. These correlations range approximately between ±0.4 as shown in Figure 5; however, if the analysis is performed using monthly averaged spectra the correlations exceed ±0.7. The changes in wave height are a response to the wind anomalies associated with PSA-1

(Figure 6b). During positive phases of PSA-1, there is an intensification of the westerly winds in the southeast Pacific sector between 40°S and 60°S and a weakening of the westerlies south of Australia. PSA-2 is strongly negatively correlated with the wave heights in the central South Pacific, reaching minimum values of <-0.4 (<-0.7 if working with monthly data). During positive phases of PSA-2, an anticlockwise circulation anomaly develops at 60°S, 120°W, which dampens the wind intensity in the South Pacific sector, diminishing the wave climate intensity in this area and across the South Pacific.

A noteworthy benefit of utilizing the approach described in section 2.2 is that it allowed us to obtain time series of changes in modeled wave direction (PC-rotation). Both PSA-1 and PSA-2 appear to have a significant impact on the rotation of the waves in the Southern Ocean. Positive phases of PSA-1 are correlated with clockwise rotations south and east of Australia and to the southwest of Chile and anticlockwise rotations in the central Pacific. Likewise, positive phases of PSA-2 are correlated with clockwise rotations around New Zealand and intense anticlockwise rotations in the eastern South Pacific. The anticlockwise and clockwise wave rotations south of Australia (identified with PSA-1 and PSA-2, respectively) could modulate changes in wave direction at the coast and hence impact or trigger dynamic processes in the South Australia sandy beaches. Previous research has highlighted the influence of SAM and ENSO on the wave climate of the Tasman Sea (e.g., Goodwin, 2005; Harley et al., 2010; Hemer et al., 2009; Ranasinghe et al., 2004). Our results show correlation values for the PSA mode indices of similar magnitude as the correlation values for NINO3.4 index for the Tasman Sea, suggesting that the PSA patterns are also important for the wave climate of this region. Therefore, these results could aid to better understand the governing physical processes that modulate the interannual variability of the wave climate in the Tasman Sea. The strong correlation values between PSA indices and PC-swell and PC-rotation in the South Pacific suggest that the wave climate at the coasts of New Zealand, Chile, and Perú could be particularly affected by this climate mode. This could have consequences in, for example, assessments of wave energy availability and extreme wave conditions in the southeast Pacific region (Mediavilla & Figueroa, 2017; Reguero et al., 2013). However, an assessment of observational wave records in these areas is necessary to confirm this relationship between the PSA modes and the wave climate.

Various other climate modes were also considered in our analysis, and their relationship with the main modes of spectral variability (swell and rotation modes) was assessed:

1. The SAM is positively correlated with Hs at high-latitudes of the Southern Ocean and in the South Pacific basin and negatively correlated in parts of the Indian and east Atlantic Oceans. The patterns of correlation are consistent with those found by Hemer et al. (2009), Izaguirre et al. (2011), and Marshall et al. (2018). The correlation with Hs decays toward the equator whereas the correlation with PC-swell is maintained in approximately the same values, since PC-swell represents the variability of only a portion of the spectrum while Hs is representative of the full wave energy contained in it. With the approach used in this study, we find that the influence of SAM extends toward the North Indian Ocean and even reaches the coasts of Baja California (~20°N). Our study suggests the SAM significantly influences the rotation of the wave field in extended areas of the Southern Hemisphere, especially southwest of Australia. This rotation is anticlockwise for positive phases of SAM, which agrees well with previous results found by Hemer et al. (2009).
2. The corresponding annular mode of the Northern Hemisphere, the AO (otherwise known as the Northern Annular Mode), shows an analogous pattern of correlation. There is a widespread negative correlation with PC-swell (and wave heights) during its positive phases, when the Northern Hemisphere storm belt contracts toward higher latitudes, generating negative zonal wind anomalies at midlatitudes. The NAO shows a very similar pattern of correlation but restricted to the North Atlantic Ocean only, and our results are in close agreement to those of previous studies that investigated the influence of the NAO on North Atlantic wave variability (e.g., Semedo et al., 2011; Woolf et al., 2002).
3. The correlation analysis with the NINO3.4 index indicates that ENSO is a major source of the signature in interannual variability in the global wave climate, with the highest influence not surprisingly in the Pacific Ocean, which is the center of action for ENSO dynamics. The distribution of the correlation coefficient between NINO3.4 and Hs agrees with that of previous studies (see, for example, Figure 3 of Izaguirre et al., 2011). El Niño events (positive NINO3.4) correspond with an increase in Hs in the North Pacific and in high-latitudes of the Indian Ocean. During La Niña (negative NINO3.4), an

increase of the wave height occurs in the southeast Pacific sector. There are some discrepancies between the Hs and PC-swell correlation distributions. For example, in the eastern equatorial Pacific, EOF-swell was selected as the mode that better correlates with the NINO3.4 index, which turned out to be the North Pacific swell. In the western equatorial Pacific, EOF-swell explains a relatively low percentage of the variance and that could be the reason for the differences with Hs in this area. As to the correlation between the NINO3.4 index and PC-rotation, it is positive in the western and southeast Pacific and negative in large areas of the eastern Pacific. This implies that El Niño events would produce a clockwise rotation of the main wave signal in most of the eastern Pacific Ocean and an anticlockwise rotation in the west. However, the correlation, although statistically significant, is generally very low with values around 0.25.

4. The PNA mode has a significant impact on the wave climate of the North Pacific: It is correlated ($R \sim 0.3$) with swell waves that are generated there and travel equatorward. The approach used in this study allows to infer that the PNA could influence the swell wave climate of the eastern equatorial Pacific. In fact, all the above-mentioned climate mode patterns appear to play respective roles in contributing to the interannual wave variability in the eastern equatorial Pacific region.

In summary, the methodology presented in this work agrees well with previous studies while at the same time allows us to better assess the potential influence of various climate modes on the components of the wave spectrum. It also helped us to better understand which of these climate patterns apparently affect the changes in wave direction (rotation). The PSA modes, previously not considered, seem to play a remarkably important influential role in the wave climate of the South Pacific, governing major changes in wave height and direction.

Data Availability Statement

The CAWCR hindcast data is available online (http://hdl.handle.net/102.100.100/137152?index=1).

Acknowledgments

The authors wish to thank the three anonymous reviewers who gave detailed comments and suggestions which helped to improve the presentation and readibility of this manuscript. The authors acknowledge the availability of the CAWCR wave hindcast, funded through the Australian Government Pacific-Australia Climate Change Science and Adaptation Program. The analysis of the data was carried out with the assistance of resources from the CSIRO High Performance Computer cluster Pearcey. EE is supported by funding from the UTAS-CSIRO Quantitative Marine Science Program, through an Institute for Marine and Antarctic Studies Tasmania Graduate Research Scholarship and a CSIRO Office of the Chief Executive top-up scholarship. EE also ackowledges support from the Australian Research Council Centre of Excellence for Climate Extremes. MH is supported by the Australian Government National Environmental Science Program Earth Systems and Climate Change (NESP ESCC) Hub. NJH acknowledges support from the Australian Research Council Centre of Excellence for Climate Extremes (Grant CE170100023) and also the NESP ESCC Hub.

References

Ardhuin, F., Rogers, E., Babanin, A. V., Filipot, J. F., Magne, R., Roland, A., et al. (2010). Semiempirical dissipation source functions for ocean waves. Part I: Definition, calibration, and validation. *Journal of Physical Oceanography*, *40*(9), 1917–1941. https://doi.org/10.1175/2010JPO4324.1

Battjes, J. A., & Janssen, J. P. F. M. (1978). Energy loss and set-up due to breaking of random waves. *Coastal Engineering*, *1978*, 569–587. https://doi.org/10.1061/9780872621909.034

Cavaleri, L., Fox-Kemper, B., & Hemer, M. (2012). Wind waves in the coupled climate system. *Bulletin of the American Meteorological Society*, *93*(11), 1651–1661. https://doi.org/10.1175/BAMS-D-11-00170.1

Deser, C., Alexander, M. A., Xie, S. P., & Phillips, A. S. (2010). Sea surface temperature variability: Patterns and mechanisms. *Annual Review of Marine Science*, *2*(1), 115–143. https://doi.org/10.1146/annurev-marine-120408-151453

Dodet, G., Mélet, A., Ardhuin, F., Bertin, X., Idier, D., & Almar, R. (2019). The contribution of wind-generated waves to coastal sea-level changes. *Surveys in Geophysics*, *40*(6), 1563–1601. https://doi.org/10.1007/s10712-019-09557-5

Durrant, T., Greenslade, D., Hemer, M., & Trenham, C. (2014). A global wave hindcast focused on the Central and South Pacific (Technical Report No. 070) The Centre for Australian Weather and Climate Research.

Durrant, T., Hemer, M., Trenham, C., & Greensdale, D. (2013a). *CAWCR Wave Hindcast Extension Jan 2011-May 2013*, *v4*. Data Collection: CSIRO. https://doi.org/10.4225/08/52817E2858340

Durrant, T., Hemer, M., Trenham, C., & Greenslade, D. (2013b). CAWCR Wave Hindcast 1979–2010 v7. Data Collection, CSIRO. https://doi.org/10.4225/08/523168703DCC5

Echevarria, E. R., Hemer, M. A., & Holbrook, N. J. (2019). Seasonal variability of the global spectral wind wave climate. *Journal of Geophysical Research: Oceans*, *124*, 2924–2939. https://doi.org/10.1029/2018JC014620

Gallet, B., & Young, W. R. (2014). Refraction of swell by surface currents. *Journal of Marine Research*, *72*(2), 105–126. https://doi.org/10.1357/002224014813758959

Gallop, S. L., Young, I. R., Ranasinghe, R., Durrant, T. H., & Haigh, I. D. (2014). The large-scale influence of the great barrier reef matrix on wave attenuation. *Coral Reefs*, *33*(4), 1167–1178. https://doi.org/10.1007/s00338-014-1205-7

Goodwin, I. D. (2005). A mid-shelf, mean wave direction climatology for southeastern Australia, and its relationship to the El Niño—Southern oscillation since 1878 AD. *International Journal of Climatology*, *25*(13), 1715–1729. https://doi.org/10.1002/joc.1207

Gulev, S. K., & Grigorieva, V. (2006). Variability of the winter wind waves and swell in the North Atlantic and North Pacific as revealed by the voluntary observing ship data. *Journal of Climate*, *19*(21), 5667–5685. https://doi.org/10.1175/JCLI3936.1

Harley, M. D., Turner, I. L., Short, A. D., & Ranasinghe, R. (2010). Interannual variability and controls of the Sydney wave climate. *International Journal of Climatology*, *30*(9), 1322–1335. https://doi.org/10.1002/joc.1962

Hasselmann, S., Hasselmann, K., Allender, J. H., & Barnett, T. P. (1985). Computations and parameterizations of the nonlinear energy transfer in a gravity-wave spectrum. Part II: Parameterizations of the nonlinear energy transfer for application in wave models. *Journal of Physical Oceanography*, *15*(11), 1378–1391. https://doi.org/10.1175/1520-0485(1985)015<1378:CAPOTN>2.0.CO;2

Hegermiller, C. A., Antolinez, J. A. A., Rueda, A., Camus, P., Perez, J., Erikson, L. H., et al. (2017). A multimodal wave spectrum–based approach for statistical downscaling of local wave climate. *Journal of Physical Oceanography*, *47*(2), 375–386. https://doi.org/10.1175/JPO-D-16-0191.1

Hemer, M. A., Church, J. A., & Hunter, J. R. (2009). Variability and trends in the directional wave climate of the Southern Hemisphere. *International Journal of Climatology*, *30*(4), 475–491. https://doi.org/10.1002/joc.1900

Hemer, M. A., Zieger, S., Durrant, T., O'Grady, J., Hoeke, R. K., McInnes, K. L., & Rosebrock, U. (2017). A revised assessment of Australia's national wave energy resource. *Renewable Energy*, *114*, 85–107. https://doi.org/10.1016/j.renene.2016.08.039

Izaguirre, C., Méndez, F. J., Menéndez, M., & Losada, I. J. (2011). Global extreme wave height variability based on satellite data. *Geophysical Research Letters*, *38*, L10607. https://doi.org/10.1029/2011GL047302

Leonard, B. P. (1979). A stable and accurate convective modelling procedure based on quadratic upstream interpolation. *Computer Methods in Applied Mechanics and Engineering*, *19*(1), 59–98. https://doi.org/10.1016/0045-7825(79)90034-3

Leonard, B. P. (1991). The ULTIMATE conservative difference scheme applied to unsteady one-dimensional advection. *Computer Methods in Applied Mechanics and Engineering*, *88*(1), 17–74. https://doi.org/10.1016/0045-7825(91)90232-U

Limpasuvan, V., & Hartmann, D. L. (1999). Eddies and the annular modes of climate variability. *Geophysical Research Letters*, *26*(20), 3133–3136. https://doi.org/10.1029/1999GL010478

Marshall, A. G., Hemer, M. A., Hendon, H. H., & McInnes, K. L. (2018). Southern annular mode impacts on global ocean surface waves. *Ocean Modelling*, *129*, 58–74. https://doi.org/10.1016/j.ocemod.2018.07.007

Marshall, A. G., Hemer, M. A., & McInnes, K. L. (2020). Australian blocking impacts on ocean surface waves. *Climate Dynamics*, *54*(3–4), 1281–1294. https://doi.org/10.1007/s00382-019-05058-8

Marshall, A. G., Hendon, H. H., Durrant, T. H., & Hemer, M. A. (2015). Madden Julian oscillation impacts on global ocean surface waves. *Ocean Modelling*, *96*, 136–147. https://doi.org/10.1016/j.ocemod.2015.06.002

Marshall, G. J., & Thompson, D. W. (2016). The signatures of large-scale patterns of atmospheric variability in Antarctic surface temperatures. *Journal of Geophysical Research: Atmospheres*, *121*, 3276–3289. https://doi.org/10.1002/2015JD024665

Marshall, G. J., Thompson, D. W., & Broeke, M. R. (2017). The signature of Southern Hemisphere atmospheric circulation patterns in Antarctic precipitation. *Geophysical Research Letters*, *44*, 11,580–11,589. https://doi.org/10.1002/2017GL075998

Mediavilla, D. G., & Figueroa, D. (2017). Assessment, sources and predictability of the swell wave power arriving to Chile. *Renewable Energy*, *114*, 108–119. https://doi.org/10.1016/j.renene.2017.03.014

Mo, K. C., & Ghil, M. (1987). Statistics and dynamics of persistent anomalies. *Journal of the Atmospheric Sciences*, *44*(5), 877–902. https://doi.org/10.1175/1520-0469(1987)044<0877:SADOPA>2.0.CO;2

Mo, K. C., & Higgins, R. W. (1998). The Pacific–South American modes and tropical convection during the Southern Hemisphere winter. *Monthly Weather Review*, *126*(6), 1581–1596. https://doi.org/10.1175/1520-0493(1998)126<1581:TPSAMA>2.0.CO;2

Mo, K. C., & Paegle, J. N. (2001). The Pacific–South American modes and their downstream effects. *International Journal of Climatology: A Journal of the Royal Meteorological Society*, *21*(10), 1211–1229. https://doi.org/10.1002/joc.685

Mortlock, T. R., & Goodwin, I. D. (2015). Directional wave climate and power variability along the Southeast Australian shelf. *Continental Shelf Research*, *98*, 36–53. https://doi.org/10.1016/j.csr.2015.02.007

Munk, W. H., & Snodgrass, F. E. (1957). Measurements of southern swell at Guadalupe Island. *Deep Sea Research*, *4*, 272–286. https://doi.org/10.1016/0146-6313(56)90061-2

Philander, S. G. H. (1983). El Nino southern oscillation phenomena. *Nature*, *302*(5906), 295–301. https://doi.org/10.1038/302295a0

Portilla-Yandún, J. (2018). The global signature of ocean wave spectra. *Geophysical Research Letters*, *45*, 267–276. https://doi.org/10.1002/2017GL076431

Portilla-Yandún, J., Salazar, A., & Cavaleri, L. (2016). Climate patterns derived from ocean wave spectra. *Geophysical Research Letters*, *43*, 11–588. https://doi.org/10.1002/2016GL071419

Preisendorfer, R. W., & Mobley, C. D. (1988). *Principal Component Analysis in Meteorology and Oceanography* (Vol. 425). Amsterdam: Elsevier.

Ranasinghe, R., McLoughlin, R., Short, A., & Symonds, G. (2004). The Southern Oscillation Index, wave climate, and beach rotation. *Marine Geology*, *204*(3–4), 273–287. https://doi.org/10.1016/S0025-3227(04)00002-7

Rapizo, H., Babanin, A. V., Schulz, E., Hemer, M. A., & Durrant, T. H. (2015). Observation of wind-waves from a moored buoy in the Southern Ocean. *Ocean Dynamics*, *65*(9–10), 1275–1288. https://doi.org/10.1007/s10236-015-0873-3

Reguero, B. G., Méndez, F. J., & Losada, I. J. (2013). Variability of multivariate wave climate in Latin America and the Caribbean. *Global and Planetary Change*, *100*, 70–84. https://doi.org/10.1016/j.gloplacha.2012.09.005

Renwick, J. A., & Revell, M. J. (1999). Blocking over the South Pacific and Rossby wave propagation. *Monthly Weather Review*, *127*(10), 2233–2247. https://doi.org/10.1175/1520-0493(1999)127<2233:BOTSPA>2.0.CO;2

Saha, S., Moorthi, S., Pan, H. L., Wu, X., Wang, J., Nadiga, S., et al. (2010). The NCEP climate forecast system reanalysis. *Bulletin of the American Meteorological Society*, *91*(8), 1015–1058. https://doi.org/10.1175/2010BAMS3001.1

Semedo, A., Sušelj, K., Rutgersson, A., & Sterl, A. (2011). A global view on the wind sea and swell climate and variability from ERA-40. *Journal of Climate*, *24*(5), 1461–1479. https://doi.org/10.1175/2010JCLI3718.1

Shimura, T., & Mori, N. (2019). High-resolution wave climate hindcast around Japan and its spectral representation. *Coastal Engineering*, *151*, 1–9. https://doi.org/10.1016/j.coastaleng.2019.04.013

Shimura, T., Mori, N., & Mase, H. (2013). Ocean waves and teleconnection patterns in the Northern Hemisphere. *Journal of Climate*, *26*(21), 8654–8670. https://doi.org/10.1175/JCLI-D-12-00397.1

Snodgrass, F. E., Hasselmann, K. F., Miller, G. R., Munk, W. H., & Powers, W. H. (1966). Propagation of ocean swell across the Pacific. *Philosophical Transactions of the Royal Society of London. Series A, Mathematical and Physical Sciences*, *259*(1103), 431–497. https://doi.org/10.1098/rsta.1966.0022

Stopa, J. E., Cheung, K. F., Tolman, H. L., & Chawla, A. (2013). Patterns and cycles in the climate forecast system reanalysis wind and wave data. *Ocean Modelling*, *70*, 207–220. https://doi.org/10.1016/j.ocemod.2012.10.005

Thompson, D. W., & Wallace, J. M. (1998). The Arctic oscillation signature in the wintertime geopotential height and temperature fields. *Geophysical Research Letters*, *25*(9), 1297–1300. https://doi.org/10.1029/98GL00950

Tolman, H. L. (2002). Alleviating the garden sprinkler effect in wind wave models. *Ocean Modelling*, *4*(3–4), 269–289. https://doi.org/10.1016/S1463-5003(02)00004-5

Tolman, H. L. (2003). Treatment of unresolved islands and ice in wind wave models. *Ocean Modelling*, *5*(3), 219–231. https://doi.org/10.1016/S1463-5003(02)00040-9

Tolman, H. L. (2009). User manual and system documentation of WAVEWATCH III TM version 3.14. *(Technical note No. 276). NOAA/NWS/NCEP/MMAB*, *276*, 220.

Wallace, J. M., & Gutzler, D. S. (1981). Teleconnections in the geopotential height field during the Northern Hemisphere winter. *Monthly Weather Review*, *109*(4), 784–812. https://doi.org/10.1175/1520-0493(1981)109<0784:TITGHF>2.0.CO;2

Wanner, H., Brönnimann, S., Casty, C., Gyalistras, D., Luterbacher, J., Schmutz, C., et al. (2001). North Atlantic oscillation–concepts and studies. *Surveys in Geophysics*, *22*(4), 321–381. https://doi.org/10.1023/A:1014217317898

Woolf, D. K., Challenor, P. G., & Cotton, P. D. (2002). Variability and predictability of the North Atlantic wave climate. *Journal of Geophysical Research*, *107*(C10), 3145. https://doi.org/10.1029/2001JC001124

Young, I. R. (1999). Seasonal variability of the global ocean wind and wave climate. *International Journal of Climatology*, *19*(9), 931–950. https://doi.org/10.1002/(SICI)1097-0088(199907)19:9<931::AID-JOC412>3.0.CO;2-O